Hindawi Publishing Corporation
International Journal of Photoenergy
Volume 2014, Article ID 823078, 10 pages
http://dx.doi.org/10.1155/2014/823078

Research Article

Layer-by-Layer Assembly and Photocatalytic Activity of Titania Nanosheets on Coal Fly Ash Microspheres

Xing Cui, Jianwen Shi, Zhilong Ye, Zhaoji Zhang, Bin Xu, and Shaohua Chen

Key Laboratory of Urban Environment and Health, Institute of Urban Environment, Chinese Academy of Sciences, Xiamen 361021, China

Correspondence should be addressed to Shaohua Chen; shchen@iue.ac.cn

Received 27 March 2014; Accepted 29 April 2014; Published 25 May 2014

Academic Editor: Jia Hong Pan

In order to address the problem with titania distribution and recovery, series of $Ti_{0.91}O_2$/CFA photocatalysts ($Ti_{0.91}O_2$/CFA-n, $n = 2, 4, 6$, and 8) were fabricated by assembling $Ti_{0.91}O_2$ nanosheets on coal fly ash (CFA) microspheres via the layer-by-layer assembly (LBLA) process and characterized by scanning electron microscopy (SEM), X-ray diffraction analysis (XRD), N_2-sorption, and ultraviolet-visible absorption (UV-vis) techniques. The SEM images and UV-vis spectra illustrated that $Ti_{0.91}O_2$ nanosheets were immobilized successfully on the CFA by the LBLA approach and changed the characteristics of CFA noticeably. The photocatalytic activity of $Ti_{0.91}O_2$/CFA was evaluated by the photodegradation of methylene blue (MB) under UV irradiation. The results demonstrated that $Ti_{0.91}O_2$/CFA-6 showed the best photocatalytic activity among the series of $Ti_{0.91}O_2$/CFA irradiated for 60 min, with a decoloration rate above 43%. After photocatalysis, the $Ti_{0.91}O_2$/CFA could be easily separated and recycled from aqueous solution and $Ti_{0.91}O_2$ nanosheets were still anchored on the CFA.

1. Introduction

Fabrication of multilayers of colloidal particles through electrostatic attraction has been studied since 1966 [1]. Generally, the composites consist of organic or inorganic particles as cores and inorganic nanocoatings as shells. For the great potentials of core-shell composites in photonics and catalysis areas, many researches have been focused on the preparation of core-shell structure via the layer-by-layer assembly (LBLA) approach in recent years [2–4]. The LBLA method has been applied to assemble charged thin films of various materials on oppositely charged templates. The inorganic coatings are deposited on the templating cores via electrostatic attraction, so the shell coatings can be adsorbed on the cores uniformly and firmly. Titanium oxide is popular with researchers for its excellent performance of high photocatalytic activity, chemical inertness, stability against photocorrosion, and cost-effectiveness [5]. Titania nanosheet ($Ti_{1-x}O_2^{4x-}$), synthesized by chemical delamination and exfoliation of precursor, is of typical 2D structure and the lateral size of it ranges from hundreds of nanometers to a few micrometers and the thickness of the individual layer is approximately 1 nm [6]. The titania nanosheets after exfoliation are negatively charged, so titania nanosheets can be assembled on substrates via the LBLA approach coupled with cationic polyelectrolyte [7]. Multilayer titania nanosheets possess unique properties besides photocatalytic activity [8], such as optical absorption properties [7, 9], high anisotropy [10], photoelectrochemical properties [11], and high thermal resistance [12].

Titania nanosheet hollow shells and hollow spheres consisting of titania and graphene nanosheets have been fabricated by the layer-by-layer assembly method in previous studies [13, 14]. However, the titania nanosheet hollow spheres are hard to separate spontaneously and recycle from aqueous suspension after photocatalysis, which limits their practical application in wastewater treatment. In order to improve the convenience of separation and recovery of nano-TiO_2, photocatalysts by immobilizing nano-TiO_2 on some substrates were recently prepared, such as on glass, polymer, and active carbon [15–17]. However, most substrate materials are expensive, and cheap and stable substrates are desired. In our early work, photocatalysts of TiO_2 immobilized on coal fly ash (CFA) were prepared [18–20]. CFA is one of the solid wastes generated from thermal power plants. CFA chosen as

a supporter has advantages as follows: (1) CFA particles are microspheres and easy to precipitate in water, so photocatalysts supported by CFA are easy to recycle from aqueous solution after reaction; (2) CFA, consisting primarily of Al_2O_3 and SiO_2, as a supporter can inhibit recombination of electron and hole effectively [21, 22]; (3) the cost of preparation and a source of environment pollution can be reduced. However, it is difficult to control uniform distribution of TiO_2 on CFA [17, 23], which greatly restrains the activity of the photocatalyst and the availability of substrate. Because the lateral size of titania nanosheets is in the micron range and CFA particle size is less than 100 μm, the problem can be solved by loading titania nanosheets on CFA through electrostatic attraction via layer-by-layer assembly method at ambient temperature [24]. The LBLA method involves electrostatic sequential deposition of negatively charged titania nanosheets onto substrate along with an oppositely charged polymer. Based on this principle, an assembly of layered titanate on CFA is expected to achieve very well.

In this paper, the titania nanosheet ($Ti_{1-x}O_2^{4x-}$) referred to is $Ti_{0.91}O_2^{0.36-}$ and is abbreviated as $Ti_{0.91}O_2$. This study describes the fabrication of $Ti_{0.91}O_2$/CFA by the LBLA approach for controlling the uniform distribution of $Ti_{0.91}O_2$. The layered $Ti_{0.91}O_2$ nanosheets were obtained by swelling and exfoliation of layered protonic titanate (γ-FeOOH type) in $(C_4H_9)_4NOH$ (TBAOH) solution and were negatively charged. The surface of CFA was modified by cationic polyelectrolyte beforehand. $Ti_{0.91}O_2$ nanosheets were adsorbed on the surface of CFA due to the electrostatic attraction and immobilized continually by repeating the LBLA procedure. $Ti_{0.91}O_2$ nanosheets anchored served as a shell and CFA could be regarded as core. The photocatalytic activity of $Ti_{0.91}O_2$/CFA was also evaluated by the decoloration of methylene blue (MB).

2. Experimental Section

2.1. Reagent and Materials. Cs_2CO_3 (99.99% metals basis), TiO_2 (AR), polyethylenimine (PEI) (99% purity) and poly(diallyldimethylammonium chloride) (PDDA) (35 wt.% aqueous solution), and TBAOH (~0.8 M) were purchased from Aladdin Reagent Company. $Ti_{0.91}O_2$ nanosheets were synthesized by a previously reported method [25]. Briefly, the protonic titanate ($H_{0.7}Ti_{1.825}O_4{\cdot}H_2O$) was prepared from cesium titanate ($Cs_{0.7}Ti_{1.825}O_4$) by acid exchange for 3 days. And then, $H_{0.7}Ti_{1.825}O_4{\cdot}H_2O$ (0.4 g) was shaken vigorously (300 rpm) in 100 mL aqueous solution of TBAOH (0.004 M) for 2 weeks, so the layered hosts underwent osmotic swelling and exfoliating into nanosheets. The colloid produced stood for storage. CFA, calcined at 800°C, was immersed in a bath of 1/1 methanol/HCl and concentrated H_2SO_4 with stirring for 20 min each and then washed with copious water to remove acid residue. The pretreated CFA was dried for use later. Deionized water was used throughout the experiments.

2.2. Fabrication Procedure. Core/shell composites (CFA was employed as a substrate core and $Ti_{0.91}O_2$ nanosheets were inorganic shell) were fabricated by electrostatic sequential deposition approach [13, 14]. For $Ti_{0.91}O_2$ nanosheets were negatively charged, in order to load $Ti_{0.91}O_2$ nanosheets onto the CFA by electrostatic deposition, the surface of CFA was modified by cationic polyelectrolytes (PEI and PDDA). The detailed fabrication procedure of layer-by-layer assembly (LBLA) method is as follows: 5 g CFA was dispersed in 200 mL PEI solution (2.5 g·L^{-1}, pH = 9) and further stirred for 60 min to ensure PEI was adsorbed on the CFA surface for introducing positive charges. After the mixture was centrifuged at 3000 rpm for 20 min, the supernatant was removed and then the CFA was washed dried in a drying oven under 60°C. Subsequently, the PEI-coated CFA (CFA/PEI) was dispersed in $Ti_{0.91}O_2$ colloidal suspension (200 mL) and further stirring was carried out for 60 min. Small flocculated aggregates formed in the solution during this process for electrostatic attraction. The resulting CFA/PEI/$Ti_{0.91}O_2$ was washed by water for 2 cycles to remove excess $Ti_{0.91}O_2$ nanosheets. After drying, it was dispersed in 200 mL PDDA solution (20 g·L^{-1}, pH = 9), as the same as the PEI modifying process, and CFA/PEI/$Ti_{0.91}O_2$/PDDA was fabricated. The procedure for PDDA/$Ti_{0.91}O_2$ alternative deposition was repeated m frequencies to synthesize a multilayer assembly-PEI/$Ti_{0.91}O_2$/$(PDDA/Ti_{0.91}O_2)_m$ (m = 1, 3, 5, and 7). In this study, the photocatalysts as-prepared were abbreviated as $Ti_{0.91}O_2$/CFA-n (n = 2, 4, 6, and 8), where n represented the loading frequency of $Ti_{0.91}O_2$ nanosheets by LBLA.

2.3. Characterizations. The morphologies of the samples were observed by a field emission scanning electron microscope (SEM) and the Ti elemental mapping was detected with an energy dispersive X-ray spectrometer (EDX) (S-4800, Japan). X-ray diffraction (XRD) data of the samples were collected using diffractometer (X'Pert PRO, Holland) with Cu Kα irradiation. The morphology of the exfoliated nanosheets was observed by transmission electron microscope (TEM, H-7650, Japan). UV-vis absorption spectra of all samples were recorded by a Shimadzu spectrophotometer (UV-2450, Japan). The chemical composition of CFA was characterized by quantitative X-ray fluorescence spectrum (XRF) analysis (Axios mAX, Holland). The N_2 adsorption-desorption isotherms, Brunauer-Emmett-Teller (BET) surface area, and Barrett-Joyner-Halenda (BJH) pore size distribution were obtained by surface area and porosity analyzer (ASAP 2020 M+C, America).

2.4. Evaluation of Photocatalytic Activity. The photocatalytic reaction was carried out in a photochemical reaction system as described before [18]. Briefly, the initial concentration and volume of MB were 20 mg/L and 50 mL, respectively. The dosage of $Ti_{0.91}O_2$/CFA-n was 0.2 g. A 500 W UV lamp with major emission at 365 nm was used as a light source, and the irradiation time was 60 min. After reaction and settling for a while, the upper solution was centrifuged at 3000 rpm for 20 min to eliminate fine particles. Then the absorbance of supernatant was analyzed at the wavelength of 664 nm by a UV-vis spectrophotometer.

3. Results and Discussion

3.1. SEM Analysis of Samples. SEM was used to define the morphology of the $Ti_{0.91}O_2$/CFA microstructure. The images present CFA before (Figures 1(a) and 1(b)) and after (Figures 1(c)–1(h)) $Ti_{0.91}O_2$ nanosheets were loaded by the LBLA approach. From Figures 1(a) and 1(b), it can be found that the surface of the CFA is smooth and barren. There are no obvious attachments on the CFA surface after rinsing with H_2SO_4 and CH_3OH, which indicates that the impurities on the surface had been removed. After $Ti_{0.91}O_2$ nanosheets were deposited on the CFA by LBLA, some aggregates consisting of $Ti_{0.91}O_2$ multilayer nanosheets were adhered to the CFA (Figures 1(c)–1(h)). With the increase of loading frequency, the area covered by corrugation was enlarged, and multilayers can be seen. It can be observed in Figure 1(c) that only very few aggregates are anchored on the surface of the CFA after twice repeated layer-by-layer loading. When the loading took place 4 times, the area of agglomerates was obviously enhanced (Figure 1(e)). Under high magnification (Figure 1(f)), there are more nanosheet agglomerates than with two loadings (Figure 1(d)). When the layer-by-layer loading frequency was further raised to 8, the agglomerates almost covered the CFA surface (Figures 1(g) and 1(h)). There is an obvious difference between the $Ti_{0.91}O_2$ nanosheet agglomerates here and the TiO_2 nanoparticle agglomerates loaded on CFA. The $Ti_{0.91}O_2$ agglomerates are of approximate rectangle sheet shape (Figure 2), and their counterparts (anatase TiO_2) are nanosphere agglomerates of 3D structure [19]. This is ascribed to the different loading methods. The conventional loading methods for fabricating TiO_2 include the sol-gel-adsorption method and the hydrothermal method [26, 27], and the TiO_2 agglomerates prepared are usually granular after calcination. In this study, the $Ti_{0.91}O_2$/CFA was fabricated without calcination under high temperature, so $Ti_{0.91}O_2$ was able to keep its original crystalline phase and did not transform into anatase or rutile. Therefore, the $Ti_{0.91}O_2$ nanosheets were still lamellar after loading on CFA. From the images of the morphology of the $Ti_{0.91}O_2$/CFA, it is certain that the $Ti_{0.91}O_2$ nanosheets are successfully immobilized on the surface of CFA with layer-by-layer approach, although the amount of $Ti_{0.91}O_2$ is smaller compared to our earlier work [19].

3.2. UV-Vis Absorption Spectra of Samples. The UV-vis absorption spectra demonstrate the optical absorption characteristics of the CFA and $Ti_{0.91}O_2$/CFA samples. In Figure 3, the absorbances of the CFA do not change much along the range of wavelengths (200 nm–800 nm), except for a weak and broad peak at around 370 nm. Compared to the spectrum of the CFA, the spectra of the $Ti_{0.91}O_2$/CFA illustrate a characteristic absorption change along the whole range of wavelengths, with two strong absorption peaks at around 266 nm and 375 nm. The peak at around 375 nm was dependent on the immobilized multilayer nanosheets which were not completely exfoliated into monolayer nanosheets. So the absorption peak has a micro red-shift. The peak of the absorption curve around 266 nm is in accord with the multilayer titania nanosheets which had been studied [7], but the absorption peak is broader than that in the study of Sasaki et al. [28]. This may be attributed to the fact that the selected substrates are different. The previous substrates were quartz glass platelets and silicon wafer chips ($1 \times 5\,cm^2$), which had a flat surface and different size from CFA. However, the substrate in this study was CFA of microsphere shape and the particle size of CFA was below 100 μm. Therefore, the assembly style of titania nanosheets on the substrate was not exactly the same. This led to the discrepancy. It can be also observed that the absorption peak of $Ti_{0.91}O_2$/CFA-6 around 266 nm is stronger than the others. It may be explained that the peak around 266 nm was previously found to be unilamellar $Ti_{0.91}O_2$ nanosheets [7], and there were more unilamellar $Ti_{0.91}O_2$ nanosheets on the surface of the CFA than other types. On $Ti_{0.91}O_2$/CFA-2, 4, 8, the incompletely exfoliated nanosheets made up a larger proportion than $Ti_{0.91}O_2$/CFA-6, which weakened the intensity of the peak around 266 nm.

3.3. Crystal Structure of Samples. XRD was used to investigate phase structure changes of the CFA before and after $Ti_{0.91}O_2$ were immobilized by LBLA. CFA and $Ti_{0.91}O_2$/CFA crystalline patterns are shown in Figures 4(a)–4(c). In Figure 4(a), CFA primarily contains mullite ($Al_{4.5}Si_{1.5}O_{9.75}$) and quartz (SiO_2), which is similar to the previous study [29]. After $Ti_{0.91}O_2$ were loaded, there was no obvious difference between CFA and $Ti_{0.91}O_2$/CFA. It could be two reasons: (1) $Ti_{0.91}O_2$ nanosheets were adhered to the surface of CFA through electrostatic force, not entering the crystal lattices of mullite and quartz; (2) the amount of deposited $Ti_{0.91}O_2$ nanosheets was small, so the influence on overall diffraction peak was little relatively. Therefore, no prominent changes in crystalline patterns of the CFA were observed clearly. However, there are still tiny differences between CFA and $Ti_{0.91}O_2$/CFA in the range of 2θ among 26°-27° (Figure 4(b)) and 39°-40° (Figure 4(c)), which are partially enlarged details of Figure 4(a). At $2\theta = 26.6°$, before $Ti_{0.91}O_2$ were loaded, the peak of the CFA is very weak; after LBLA was carried out for several frequencies, there is a small peak, which is higher than the CFA sample. At $2\theta = 39.5°$, the intensity of the CFA peak decreases remarkably after $Ti_{0.91}O_2$ were immobilized. Figure 4(d) depicts the XRD pattern of protonic titanate before exfoliation. The peak at 9.5° is a characteristic of protonic titanate, and it disappears on $Ti_{0.91}O_2$/CFA, which can prove that slight changes of $Ti_{0.91}O_2$/CFA XRD pattern at $2\theta = 26.6°$ and 39.5° resulted from the loaded titania nanosheets via LBLA, not protonic titanate. This confirms that LBLA method is feasible to immobilize $Ti_{0.91}O_2$ nanosheets.

3.4. N_2 Adsorption-Desorption and Pore Distribution of Samples. The BET surface area of the $Ti_{0.91}O_2$/CFA as-prepared is summarized in Table 2. Before $Ti_{0.91}O_2$ were loaded, the BET surface area of CFA was 2.62 m^2/g. After $Ti_{0.91}O_2$ nanosheets were loaded, the BET surface area of $Ti_{0.91}O_2$/CFA-2 declined instead, so did the surface area of $Ti_{0.91}O_2$/CFA-4. When the loading frequency was 6, the specific surface area of $Ti_{0.91}O_2$/CFA-6 reduced to the minimum which is about

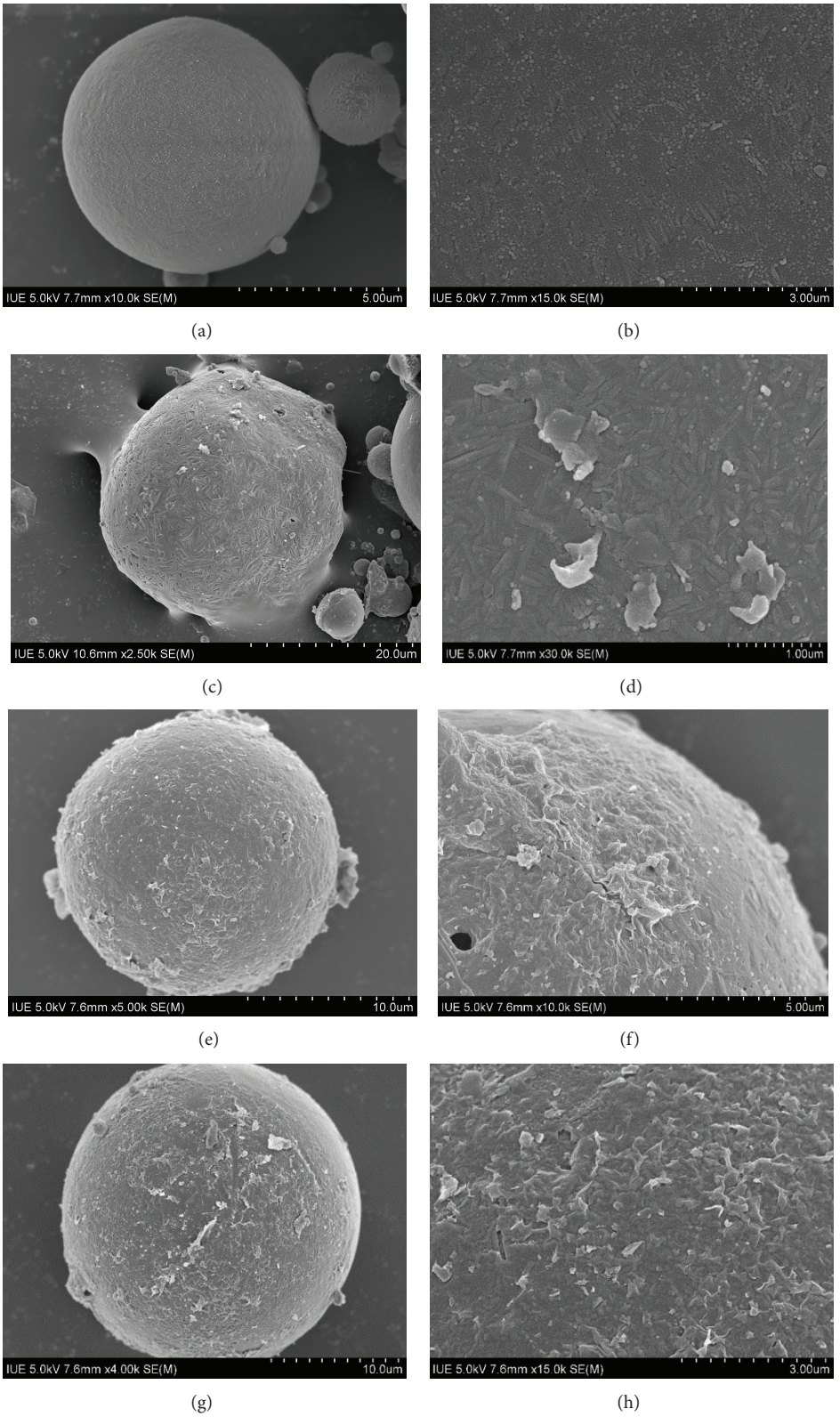

Figure 1: The SEM images of samples as-prepared: (a) and (b) CFA; (c) and (d) $Ti_{0.91}O_2$/CFA-2; (e) and (f) $Ti_{0.91}O_2$/CFA-4; (g) and (h) $Ti_{0.91}O_2$/CFA-8.

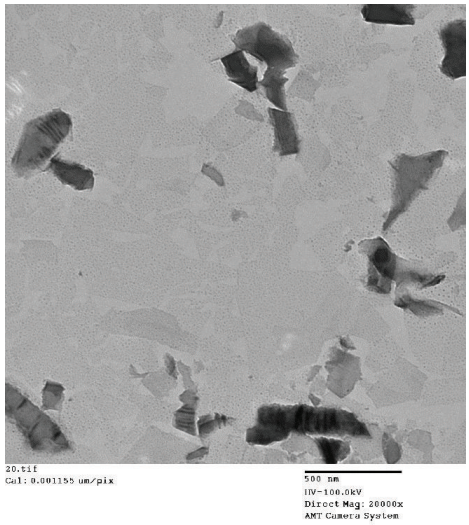

Figure 2: TEM of exfoliated titania nanosheets.

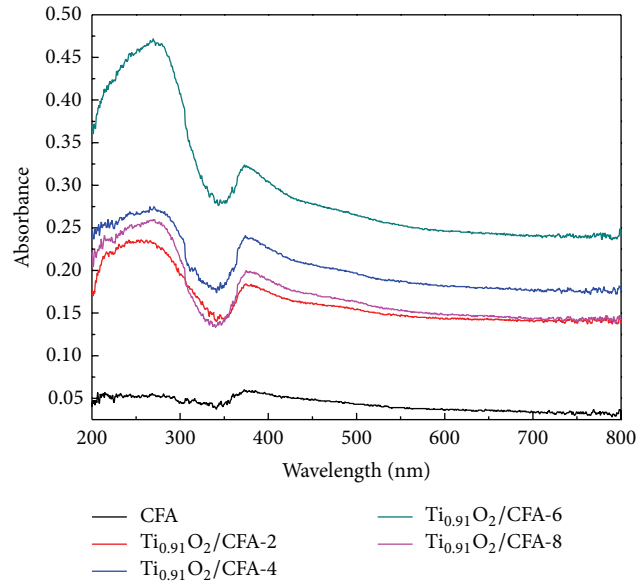

Figure 3: UV-vis absorption spectra of CFA and $Ti_{0.91}O_2$/CFA.

1.26 m^2/g; the specific surface area increases slightly while the loading frequency rose to 8, however, still below 2 m^2/g. The specific surface area decreased gradually with the increase in loading $Ti_{0.91}O_2$ nanosheets, similar to the results reported previously [30, 31]. The reason may be that $Ti_{0.91}O_2$ nanosheets immobilized by LBLA on the surface of the CFA were a few and lamellar, so it was difficult to form porous structure, which could not change the surface area much. The specific surface area of $Ti_{0.91}O_2$/CFA-6 was the smallest among the samples. Combined with UV-vis absorption analysis, this can be attributed to the monolayer nanosheets. Unilamellar $Ti_{0.91}O_2$ nanosheets were loaded more regularly than multilayer (incompletely exfoliated nanosheets) on the surface of CFA, so the surface structure of $Ti_{0.91}O_2$/CFA-6 is less complicated than others with a smaller surface area.

Figure 5 shows the N_2 adsorption-desorption isotherms of CFA and $Ti_{0.91}O_2$/CFA samples. It can be seen that all the samples can be assigned as an isotherm of type 2 in the IUPAC classification [32, 33]. The fact that the hysteresis loop is difficult to observe and volume adsorbed is very small reveals that the samples are typically nonporous characteristic by LBLA [34]. Moreover, it is shown that the adsorption capacity of the $Ti_{0.91}O_2$/CFA is lower than the CFA. With the loaded $Ti_{0.91}O_2$ nanosheets increasing, adsorption capacity and the hysteresis loop of $Ti_{0.91}O_2$/CFA became low and small gradually, respectively, which implies that immobilization of $Ti_{0.91}O_2$ nanosheets resulted in forming new structure (not 3D network), but did not increase the pore volume.

The pore size distribution of the CFA and $Ti_{0.91}O_2$/CFA in Figure 6 illustrates that pores of all samples are micropores and mesopores in a wide distribution range (<2 nm to 50 nm). Pores below 3 nm of all samples take a large amount with small pore volume. This can be explained by the fact that the specific surface area was very small and the samples were nearly nonporous. After $Ti_{0.91}O_2$ nanosheets were anchored by LBLA on CFA, the mesopore distribution of the $Ti_{0.91}O_2$/CFA samples slightly shifts to 18 nm compared with 15 nm of the CFA, and the specific surface area of $Ti_{0.91}O_2$/CFA drops correspondingly. However, $Ti_{0.91}O_2$ nanosheets did not change the pore size distribution much either.

The results above of BET surface area, N_2 adsorption-desorption isotherms, and pore size distribution demonstrate that the loaded $Ti_{0.91}O_2$ by LBLA do not change the pore structure of the CFA. It is ascribed to $Ti_{0.91}O_2$ nanosheets which are lamellar with general lateral size of submicrons to microns and unilamellar thickness of ~1 nm. In this study, the lateral size of $Ti_{0.91}O_2$ nanosheets presented in Figure 2 is in the range of 200 nm–500 nm. The nanosheets are bigger than the pores of CFA and can cover them. However, the particle diameter of the CFA was above 5 μm and greatly larger than the size of $Ti_{0.91}O_2$ nanosheets, so $Ti_{0.91}O_2$ nanosheets stacked on the surface of CFA closely to form new structure but cannot fundamentally change the architecture of CFA. This conclusion is further supported by the image magnification of the $Ti_{0.91}O_2$/CFA in Figure 1.

3.5. Photocatalytic Activity. The photocatalytic activity of $Ti_{0.91}O_2$/CFA was investigated by the degradation of MB solution as a test reaction. Blank experiment (MB solution without CFA and $Ti_{0.91}O_2$/CFA) was served as a comparison. Before the photocatalytic reaction began, the adsorption experiment in the dark lasted for 60 min to reach adsorption equilibrium [35]. The absorbance of MB is proportional to its concentration, so the decoloration rate can be calculated by the equation as follows: $\eta(\%) = 100(A_0 - A_t)/A_0\% = 100(C_0 - C_t)/C_0\%$, where A_0 and A_t are the absorbances of MB solution at initial and t time, respectively.

Figure 7(a) shows MB was eliminated only ~10% by adsorption of samples and did not degrade in the blank experiment when the UV light was switched off. When the

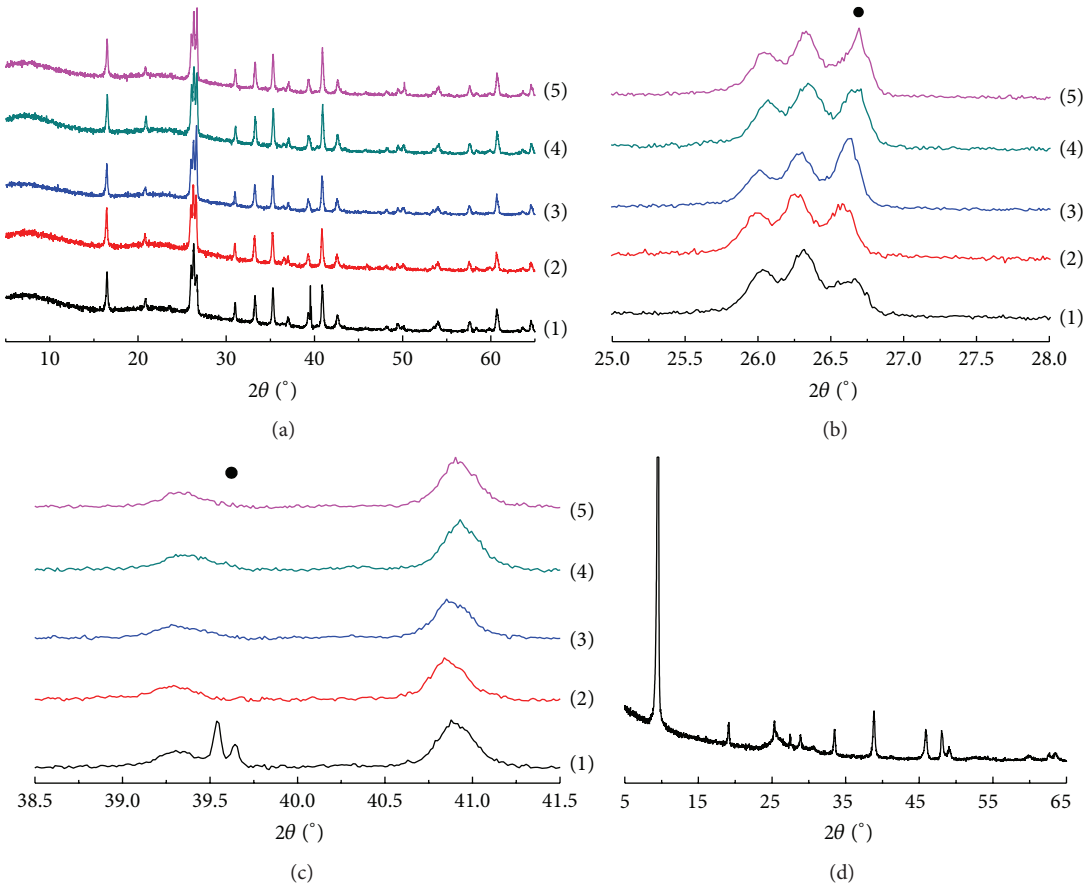

Figure 4: XRD patterns of (a–c) CFA and $Ti_{0.91}O_2$/CFA samples and (d) protonic titanate: (1) CFA; (2) $Ti_{0.91}O_2$/CFA-2; (3) $Ti_{0.91}O_2$/CFA-4; (4) $Ti_{0.91}O_2$/CFA-6; (5) $Ti_{0.91}O_2$/CFA-8.

Table 1: The chemical composition of CFA (wt.%).

Al_2O_3	SiO_2	Fe_2O_3	CaO	TiO_2	K_2O	Others
35.8	54.7	2.52	1.74	1.32	1.17	2.75

UV light was on, the MB degraded rapidly. In the initial 10 min, the decoloration efficiencies of $Ti_{0.91}O_2$/CFA-*n* are almost equivalent to that during 1 h adsorption without UV irradiation. The concentration of MB decreases further with the prolonged UV light. After 60 min of photocatalysis reaction, the concentration of MB reduces to half of the initial. Figure 7(b) displays the decoloration rates of all the samples after 60 min UV light illumination. It can be seen that the removal efficiency of blank is much lower than that of the CFA and $Ti_{0.91}O_2$/CFA. This indicates that MB is removed through photocatalysis primarily under UV irradiation, not photolysis. Meanwhile, all $Ti_{0.91}O_2$/CFA samples have higher decoloration rate above 24% than CFA which is about 15%. A poor photocatalytic characteristic of CFA originated from its chemical component (Table 1), which was the same as our early work [18], so $Ti_{0.91}O_2$ contributes to photocatalytic activity principally. This demonstrates again that it is successful to load $Ti_{0.91}O_2$ nanosheets on CFA via LBLA.

Generally, the photocatalytic activity is enhanced with increasing the $Ti_{0.91}O_2$ layer-by-layer loading frequency. With two frequencies loading, the decoloration rate of the $Ti_{0.91}O_2$/CFA-2 achieved 24.7% correspondingly; when $Ti_{0.91}O_2$ loading accomplished 4 frequencies, the photocatalytic activity of the $Ti_{0.91}O_2$/CFA improved remarkably, with a decoloration rate of 41.8%, due to more $Ti_{0.91}O_2$ nanosheets immobilized. While the loading frequency was raised to 6 further, the activity improved a little, up to a maximum decoloration rate about 43.2%. Nevertheless, the activity of $Ti_{0.91}O_2$/CFA-8 was lower than $Ti_{0.91}O_2$/CFA-4, 6. It is understandable that the amount of $Ti_{0.91}O_2$ nanosheets anchored on CFA influences the photocatalytic activity. The more $Ti_{0.91}O_2$ nanosheets were loaded, the higher activity the sample had. However, the excessive $Ti_{0.91}O_2$ nanosheets would block the UV illumination into the interior of photocatalyst, with a depressed availability of UV irradiation, which was consistent with other studies [36–38]. Meanwhile, the transfer of charge carrier may be also limited. It should be noted that $Ti_{0.91}O_2$/CFA-6 exhibited the highest photocatalytic activity whose specific surface area and pore volume are the smallest. It may be also explained that there are more $Ti_{0.91}O_2$ monolayer nanosheets (with high photocatalytic activity by themselves and not blocking UV illumination) on the surface of $Ti_{0.91}O_2$/CFA-6 than others for its UV absorbance spectral

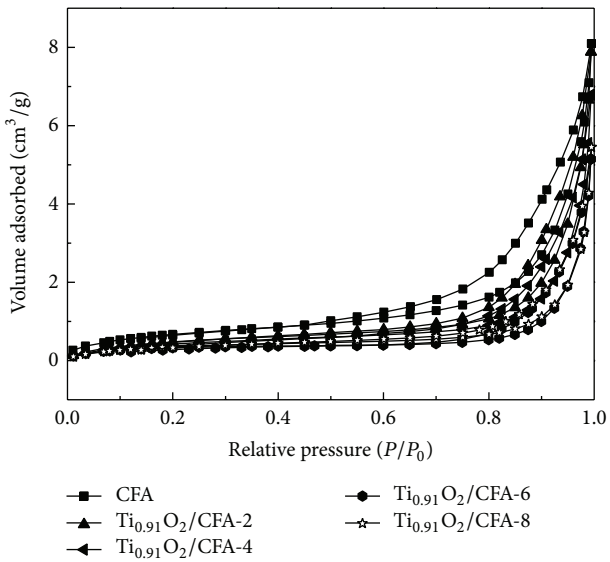

Figure 5: Nitrogen adsorption-desorption isotherms of CFA and $Ti_{0.91}O_2$/CFA.

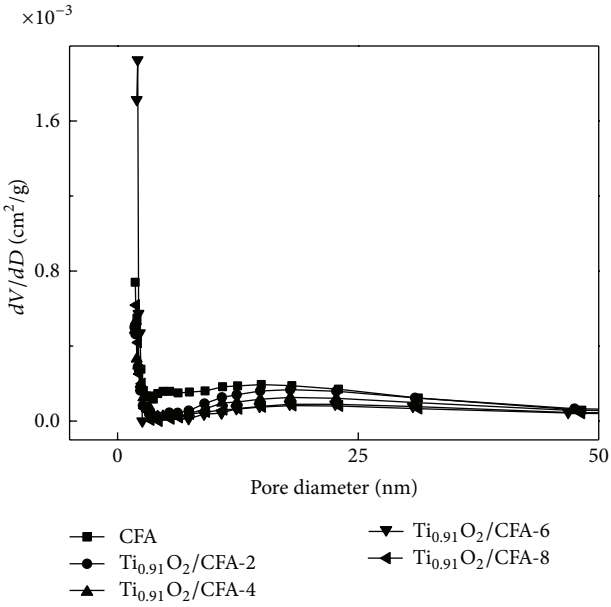

Figure 6: Pore size distributions of CFA and $Ti_{0.91}O_2$/CFA.

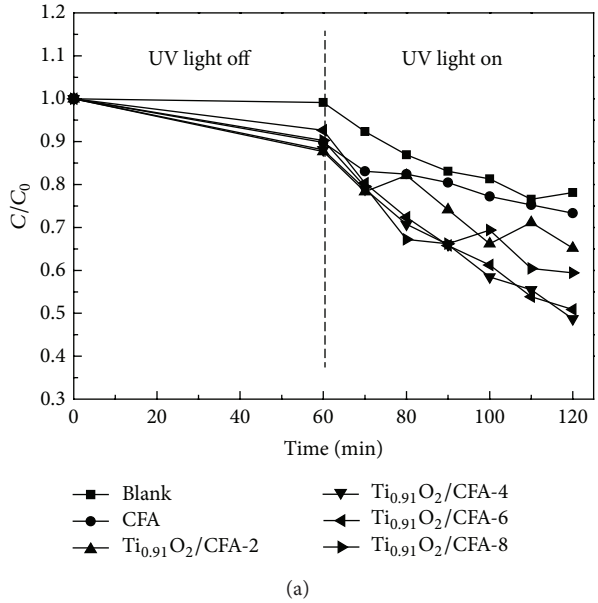

(a)

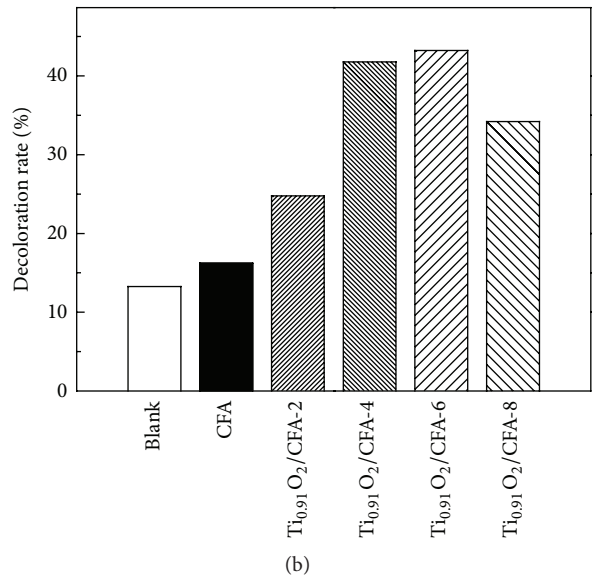

(b)

Figure 7: Photocatalytic activities of all samples.

profile with a stronger peak at 266 nm, which had been discussed in UV-vis and BET analysis. Although the decoloration rate (43.2%) was not too high when $Ti_{0.91}O_2$/CFA-*n* were used as photocatalysts, $Ti_{0.91}O_2$/CFA-*n* are very easy to separate and recycle from aqueous suspension due to the weight of CFA, which facilitates the recycle and reuse, as mentioned in our previous publication [18–20].

Figure 8 illustrates the SEM and EDX micrographs of the $Ti_{0.91}O_2$/CFA-6 before (Figures 8(a) and 8(b)) and after photocatalysis (Figures 8(c) and 8(d)). It is obvious that there are almost no changes in the appearance of $Ti_{0.91}O_2$/CFA-6, and $Ti_{0.91}O_2$ nanosheets can be still found on the surface of CFA microspheres with a considerable amount, which suggests that $Ti_{0.91}O_2$ nanosheets can stick to CFA firmly through the LBLA method. From Figure 8(d), the enlargement of Figure 8(c), it is observed that the morphology of $Ti_{0.91}O_2$ nanosheets changes a little. The edge of certain $Ti_{0.91}O_2$ nanosheets bends slightly, called "warping," which may be ascribed to the illumination of UV-light [8, 39]. However, this did not influence the stability for their partial existences on the surface of substrate. Figure 8(f) is the Ti mapping of $Ti_{0.91}O_2$/CFA as presented in Figure 8(e) which shows the distribution of Ti-containing species on the surface of CFA microsphere. This indicates that there is another difference between $Ti_{0.91}O_2$/CFA and conventional TiO_2 cluster immobilized on substrates. In conventional studies, it was difficult to control TiO_2 cluster loaded on

Table 2: BET surface area and pore volume of CFA and $Ti_{0.91}O_2$/CFA.

Samples	CFA	$Ti_{0.91}O_2$/CFA-2	$Ti_{0.91}O_2$/CFA-4	$Ti_{0.91}O_2$/CFA-6	$Ti_{0.91}O_2$/CFA-8	TBA-intercalated layered titanate [42]
S_{BET} (m^2/g)	2.62	1.94	1.72	1.26	1.41	24
Pore volume (cm^3/g) × 10^3	12.6	12.2	10.6	7.9	8.5	0

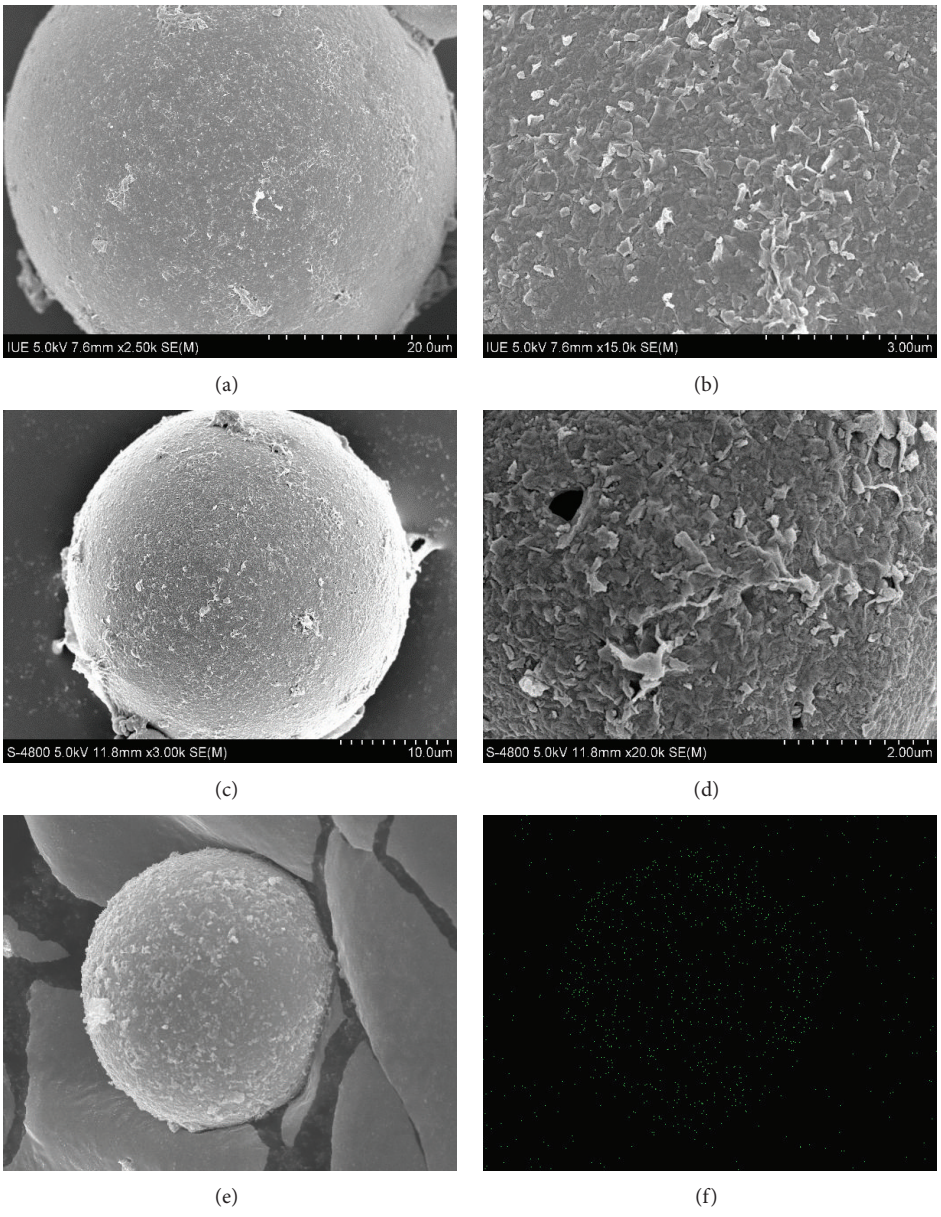

Figure 8: SEM images and EDX analysis of $Ti_{0.91}O_2$/CFA-6: (a) and (b) sample as-prepared; (c) and (d) sample after photocatalysis; (e) and (f) Ti mapping of sample.

supporters uniformly [40, 41]. However, from $Ti_{0.91}O_2$/CFA as-prepared in our work, it can be seen that Ti element is well-distributed, which can improve the availability of substrate. It is a unique feature of $Ti_{0.91}O_2$/CFA. In a word, the unilamellar nanosheets can be easily and compactly immobilized on the CFA by LBLA, which is in favor of maintaining the stability of $Ti_{0.91}O_2$/CFA.

4. Conclusion

We fabricated a novel photocatalyst successfully via the layer-by-layer assembly method. $Ti_{0.91}O_2$ nanosheets were immobilized on CFA by using sequential modification of cationic polyelectrolyte and $Ti_{0.91}O_2$ nanosheets. Since $Ti_{0.91}O_2$ nanosheets have special properties, $Ti_{0.91}O_2$/CFA

exhibits different characteristics, which can be concluded as follows.

(1) Difference in morphology depends on the loading frequency. The amount of $Ti_{0.91}O_2$ nanosheets on the CFA surface increases with the layer-by-layer assembly frequency increasing. $Ti_{0.91}O_2$ nanosheets distribute uniformly on the surface of CFA whose availability can be improved.

(2) CFA exhibits weak optical absorption in whole range of wavelength compared with $Ti_{0.91}O_2$/CFA, which proves that the immobilization of $Ti_{0.91}O_2$ nanosheets by LBLA can enhance the UV-absorption of the CFA. $Ti_{0.91}O_2$/CFA has a UV-absorption peak around 266 nm.

(3) $Ti_{0.91}O_2$/CFA shows photocatalytic activity. Significant enhancement in decoloration of MB can be achieved by $Ti_{0.91}O_2$/CFA compared to barren CFA. $Ti_{0.91}O_2$/CFA is also easy to recycle and of mechanical stability, causing little secondary pollution.

Conflict of Interests

The authors declare that there is no conflict of interests regarding the publication of this paper.

Acknowledgments

This work was supported by Key Project of Science and Technology Plan of Fujian Province (no. 2012Y0066); National Key Technology Support Program (2012BAC25B04); Science and Technology Major Project of Fujian Province (2013YZ0001-1). We thank Professor M. L. Fu and Dr. J. W. Chen for their kind help.

References

[1] R. K. Iler, "Multilayers of colloidal particles," *Journal of Colloid And Interface Science*, vol. 21, no. 6, pp. 569–594, 1966.

[2] G. Decher, "Fuzzy nanoassemblies: toward layered polymeric multicomposites," *Science*, vol. 277, pp. 1232–1237, 1997.

[3] F. Caruso, R. A. Caruso, and H. Möhwald, "Nanoengineering of inorganic and hybrid hollow spheres by colloidal templating," *Science*, vol. 282, no. 5391, pp. 1111–1114, 1998.

[4] F. Caruso, X. Shi, R. Caruso, and A. Susha, "Hollow titania spheres from layered precursor deposition on sacrificial colloidal core particles," *Advanced Materials*, vol. 13, pp. 740–744, 2001.

[5] J. H. Pan, H. Dou, Z. Xiong, C. Xu, J. Ma, and X. S. Zhao, "Porous photocatalysts for advanced water purifications," *Journal of Materials Chemistry*, vol. 20, no. 22, pp. 4512–4528, 2010.

[6] R. Ma and T. Sasaki, "Nanosheets of oxides and hydroxides: ultimate 2D charge-bearing functional crystallites," *Advanced Materials*, vol. 22, no. 45, pp. 5082–5104, 2010.

[7] T. Sasaki, Y. Ebina, M. Watanabe, and G. Decher, "Multilayer ultrathin films of molecular titania nanosheets showing highly efficient UV-light absorption," *Chemical Communications*, no. 21, pp. 2163–2164, 2000.

[8] T. Shibata, N. Sakai, K. Fukuda, Y. Ebina, and T. Sasaki, "Photocatalytic properties of titania nanostructured films fabricated from titania nanosheets," *Physical Chemistry Chemical Physics*, vol. 9, no. 19, pp. 2413–2420, 2007.

[9] T. Sasaki and M. Watanabe, "Semiconductor nanosheet crystallites of quasi-TiO_2 and their optical properties," *The Journal of Physical Chemistry B*, vol. 101, pp. 10159–10161, 1997.

[10] T. Maluangnont, K. Matsuba, F. Geng, R. Ma, Y. Yamauchi, and T. Sasaki, "Osmotic swelling of layered compounds as a route to producing high-quality two-dimensional materials. A comparative study of tetramethylammonium versus tetrabutylammonium cation in a lepidocrocite-type titanate," *Chemistry of Materials*, vol. 25, pp. 3137–3146, 2013.

[11] N. Sakai, Y. Ebina, K. Takada, and T. Sasaki, "Electronic band structure of titania semiconductor nanosheets revealed by electrochemical and photoelectrochemical studies," *Journal of the American Chemical Society*, vol. 126, no. 18, pp. 5851–5858, 2004.

[12] K. Fukuda, Y. Ebina, T. Shibata, T. Aizawa, I. Nakai, and T. Sasaki, "Unusual crystallization behaviors of anatase nanocrystallites from a molecularly thin titania nanosheet and its stacked forms: increase in nucleation temperature and oriented growth," *Journal of the American Chemical Society*, vol. 129, no. 1, pp. 202–209, 2007.

[13] L. Wang, T. Sasaki, Y. Ebina, K. Kurashima, and M. Watanabe, "Fabrication of controllable ultrathin hollow shells by layer-by-layer assembly of exfoliated titania nanosheets on polymer templates," *Chemistry of Materials*, vol. 14, no. 11, pp. 4827–4832, 2002.

[14] W. Tu, Y. Zhou, Q. Liu et al., "Robust hollow spheres consisting of alternating titania nanosheets and graphene nanosheets with high photocatalytic activity for CO_2 conversion into renewable fuels," *Advanced Functional Materials*, vol. 22, no. 6, pp. 1215–1221, 2012.

[15] D. Robert, A. Piscopo, O. Heintz, and J. V. Weber, "Photocatalytic detoxification with TiO_2 supported on glass-fibre by using artificial and natural light," *Catalysis Today*, vol. 54, no. 2-3, pp. 291–296, 1999.

[16] M. E. Fabiyi and R. L. Skelton, "Photocatalytic mineralisation of methylene blue using buoyant TiO_2-coated polystyrene beads," *Journal of Photochemistry and Photobiology A: Chemistry*, vol. 132, no. 1-2, pp. 121–128, 2000.

[17] B. Gao, P. S. Yap, T. M. Lim, and T.-T. Lim, "Adsorption-photocatalytic degradation of Acid Red 88 by supported TiO_2: effect of activated carbon support and aqueous anions," *Chemical Engineering Journal*, vol. 171, no. 3, pp. 1098–1107, 2011.

[18] J. Shi, S. Chen, S. Wang, P. Wu, and G. Xu, "Favorable recycling photocatalyst TiO_2/CFA: effects of loading method on the structural property and photocatalytic activity," *Journal of Molecular Catalysis A: Chemical*, vol. 303, pp. 141–147, 2009.

[19] J. Shi, S. Chen, Z. Ye, S. Wang, and P. Wu, "Favorable recycling photocatalyst TiO_2/CFA: effects of loading percent of TiO_2 on the structural property and photocatalytic activity," *Applied Surface Science*, vol. 257, pp. 1068–1074, 2010.

[20] J. Shi, S. Chen, S. Wang, Z. Ye, P. Wu, and B. Xu, "Favorable recycling photocatalyst TiO_2/CFA: effects of calcination temperature on the structural property and photocatalytic activity," *Journal of Molecular Catalysis A: Chemical*, vol. 330, pp. 41–448, 2010.

[21] D. Zhao, C. Chen, Y. Wang et al., "Enhanced photocatalytic degradation of dye pollutants under visible irradiation on Al(III)-modified TiO_2: structure, interaction, and interfacial

electron transfer," *Environmental Science and Technology*, vol. 42, no. 1, pp. 308–314, 2008.

[22] W. Kim, T. Tachikawa, T. Majima, and W. Choi, "Photocatalysis of dye-sensitized TiO_2 nanoparticles with thin overcoat of Al_2O_3: enhanced activity for H_2 production and dechlorination of CCl_4 ," *Journal of Physical Chemistry C*, vol. 113, no. 24, pp. 10603–10609, 2009.

[23] Y.-T. Yu, "Preparation of nanocrystalline TiO_2-coated coal fly ash and effect of iron oxides in coal fly ash on photocatalytic activity," *Powder Technology*, vol. 146, no. 1-2, pp. 154–159, 2004.

[24] T. Sasaki, Y. Ebina, T. Tanaka, M. Harada, M. Watanabe, and G. Decher, "Layer-by-layer assembly of titania nanosheet/polycation composite films," *Chemistry of Materials*, vol. 13, no. 12, pp. 4661–4667, 2001.

[25] T. Sasaki and M. Watanabe, "Osmotic swelling to exfoliation. Exceptionally high degrees of hydration of a layered titanate," *Journal of the American Chemical Society*, vol. 120, no. 19, pp. 4682–4689, 1998.

[26] Y. Li, M. Guo, M. Zhang, and X. Wang, "Hydrothermal synthesis and characterization of TiO_2 nanorod arrays on glass substrates," *Materials Research Bulletin*, vol. 44, no. 6, pp. 1232–1237, 2009.

[27] J. Shi, J. Zheng, P. Wu, and X. Ji, "Immobilization of TiO_2 films on activated carbon fiber and their photocatalytic degradation properties for dye compounds with different molecular size," *Catalysis Communications*, vol. 9, no. 9, pp. 1846–1850, 2008.

[28] T. Sasaki, Y. Ebina, K. Fukuda, T. Tanaka, M. Harada, and M. Watanabe, "Titania nanostructured films derived from a titania nanosheet/polycation multilayer assembly via heat treatment and UV irradiation," *Chemistry of Materials*, vol. 14, no. 8, pp. 3524–3530, 2002.

[29] K. Xu, T. Deng, J. Liu, and W. Peng, "Study on the phosphate removal from aqueous solution using modified fly ash," *Fuel*, vol. 89, no. 12, pp. 3668–3674, 2010.

[30] X. Wang, Y. Liu, Z. Hu, Y. Chen, W. Liu, and G. Zhao, "Degradation of methyl orange by composite photocatalysts nano-TiO_2 immobilized on activated carbons of different porosities," *Journal of Hazardous Materials*, vol. 169, no. 1–3, pp. 1061–1067, 2009.

[31] H. Nishikiori, M. Furukawa, and T. Fujii, "Degradation of trichloroethylene using highly adsorptive allophane-TiO_2 nanocomposite," *Applied Catalysis B: Environmental*, vol. 102, no. 3-4, pp. 470–474, 2011.

[32] G. SJ and K. Sing, *Adsorption, Surface Area and Porosity*, Academic Press, London, UK, 1982.

[33] Y. Zhang, D. Wang, and G. Zhang, "Photocatalytic degradation of organic contaminants by TiO_2/sepiolite composites prepared at low temperature," *Chemical Engineering Journal*, vol. 173, no. 1, pp. 1–10, 2011.

[34] J. Yu, Y. Su, and B. Cheng, "Template-free fabrication and enhanced photocatalytic activity of hierarchical Macro/Mesoporous titania," *Advanced Functional Materials*, vol. 17, pp. 1984–1990, 2007.

[35] F. Chen, Z. Liu, Y. Liu, P. Fang, and Y. Dai, "Enhanced adsorption and photocatalytic degradation of high-concentration methylene blue on Ag_2O-modified TiO_2-based nanosheet," *Chemical Engineering Journal*, vol. 221, pp. 283–291, 2013.

[36] T. A. McMurray, J. A. Byrne, P. S. M. Dunlop, J. G. M. Winkelman, B. R. Eggins, and E. T. McAdams, "Intrinsic kinetics of photocatalytic oxidation of formic and oxalic acid on immobilised TiO_2 films," *Applied Catalysis A: General*, vol. 262, no. 1, pp. 105–110, 2004.

[37] H. T. Chang, N.-M. Wu, and F. Zhu, "A kinetic model for photocatalytic degradation of organic contaminants in a thin-film TiO_2 catalyst," *Water Research*, vol. 34, no. 2, pp. 407–416, 2000.

[38] J.-M. Lee, M.-S. Kim, and B.-W. Kim, "Photodegradation of bisphenol-A with TiO_2 immobilized on the glass tubes including the UV light lamps," *Water Research*, vol. 38, no. 16, pp. 3605–3613, 2004.

[39] N. Sakai, A. Fujishima, T. Watanabe, and K. Hashimoto, "Quantitative evaluation of the photoinduced hydrophilic conversion properties of TiO_2 thin film surfaces by the reciprocal of contact angle," *Journal of Physical Chemistry B*, vol. 107, no. 4, pp. 1028–1035, 2003.

[40] Y. Xu, B. Lei, L. Guo, W. Zhou, and Y. Liu, "Preparation, characterization and photocatalytic activity of manganese doped TiO_2 immobilized on silica gel," *Journal of Hazardous Materials*, vol. 160, no. 1, pp. 78–82, 2008.

[41] R. Yuan, R. Guan, W. Shen, and J. Zheng, "Photocatalytic degradation of methylene blue by a combination of TiO_2 and activated carbon fibers," *Journal of Colloid and Interface Science*, vol. 282, no. 1, pp. 87–91, 2005.

[42] J.-H. Choy, H.-C. Lee, H. Jung, H. Kim, and H. Boo, "Exfoliation and restacking route to anatase-layered titanate nanohybrid with enhanced photocatalytic activity," *Chemistry of Materials*, vol. 14, no. 6, pp. 2486–2491, 2002.